Statistical Analysis and Modeling of User Micromobility for THz Cellular Communications

Nikita Stepanov, Dmitri Moltchanov, Vyacheslav Begishev,
Andrey Turlikov, and Yevgeni Koucheryavy, *Senior Member, IEEE*

***Abstract*—Terahertz (THz, $0.3-3$ THz) wireless access is nowadays considered as a major enabling technology for sixth generation (6G) cellular systems. To compensate for high propagation losses, these systems will utilize antenna arrays with extremely directional beams. The performance of such systems will thus be heavily affected by micromobility such as shakes and rotations of user equipment (UE) even when user is in stationary position. The ultimate impact of micromobility is spontaneous degradation of signal-to-noise (SNR) level leading to outages. In this paper, we measure and statistically investigate the micromobility process of various applications including video viewing, phone calling, virtual reality viewing and racing game. Particularly, we characterize occupancy distributions and first-passage time (FPT) to outage for various antenna configurations. We also assess the radial symmetry in micromobility patterns and characterize distance-dependent velocity and drift to the origin parameters. The obtained results are essential for developing mathematical models of micromobility patterns that needs to be further used in system-level analysis of THz cellular systems. To this end, we also illustrate that Markov models are only suitable for applications with low and purely random micromobility dynamics such as video viewing and phone calling. When a user is controlled by the application, as in the case of gaming, Markov models overestimate FPT to outage.**

***Index Terms*—6G, terahertz, micromobility, measurements, applications, statistical analysis, outage**

I. Introduction

Terahertz (THz) communications systems operating in $0.3-3$ THz band are expected to become one of the major steps towards sixth generation (6G) cellular systems [1], [2]. The extreme amount of spectrum available in this band will enable principally new applications at the air interface such as holographic communications, augmented and virtual reality as well as tactile communications [3], [4].

However, in addition to these promises THz band is characterized by a unique set of challenges that have to be addressed with severe path loss being one of the most critical [5], [6]. To compensate for these losses [7], antenna arrays having hundreds or even thousands of elements are expected to be utilized at a base station (BS) side [8]. These antennas will form extremely directional radiation patterns of just one degree and even less. Although such exceptional beamwidths would allow to efficiently reduce interference and greatly expand the coverage range of BSs [9], they also bring a unique negative impact on the stability of THz links. Particularly, in such systems not only large-scale mobility may lead to the loss of connectivity but user micromobility as well, i.e., spontaneous turns and displacements that unavoidably happen to mobile user equipment (UE) even when user is stationary [10].

The effect of micromobility of THz communications has been first revealed in [10], where the authors proposed empirical models for user mobility for few applications including mobile gaming and phone calling. However, the mobility patterns have been measured using smartphones' embedded motion sensors that are known to introduce significant errors due to the inertial nature of the measurement system. The micromobility modelling and associated performance evaluation of THz link capacity and outage probability have been performed in [11]. However, the authors assume several simplifications making the analysis feasible including the Brownian nature of micromobility patterns and independence of mobility components over different axes. Furthermore, the model is not based on statistical data that may also lead to biased conclusions. The micromobility has also been recently studied in the context of mmWave UAV communication systems [12], [13] and also mentioned as one of the sources for outages in case of THz backhaul systems [14], [15]. However, the micromobility patterns in these systems are affected by drastically different sources of randomness and thus do not apply to the case of cellular communications.

In this paper, we perform an extensive measurement campaign of stochastic user micromobility patterns for four different classes of applications: (i) video viewing, (ii) phone calling, (iii) virtual reality (VR) viewing, and (iv) race gaming. To increase the accuracy of the presented results, we adopt direct measurements methodology efficiently avoiding errors associated with the use of inertial systems. We then proceed analyzing the measured mobility patterns including the first passage time (FPT) to the circular boundary characterizing uninterrupted connectivity time (i.e., time to outage). Further, by setting the aim for mathematical micromobility modelling for performance evaluation of THz communication systems, we provide an in-depth analysis of statistical characteristics of micromobility patterns. Finally, we develop Markov models for all the considered applications and assess their accuracy.

The main contributions of our study are:

- to support the design of THz cellular systems, we perform

N. Stepanov and A. Turlikov are with Saint-Petersburg State University of Aerospace Instrumentation (GUAP University), St-Petersburg, Russia, E-mail: stepanov.nikita@guap.ru, turlikov@guap.ru.

D. Moltchanov and Y. Koucheryavy are with Tampere University, Finland. Email: firstname.lastname@tuni.fi.

V. Begishev is with Peoples' Friendship University of Russia (RUDN University), Moscow, Russia. Email: begishev-vo@rudn.ru.

Yevgeni Koucheryavy is also with Higher School of Economics, National Research University, Moscow, Russia.

The research was funded by the Russian Science Foundation, project no. 21-79-10139.

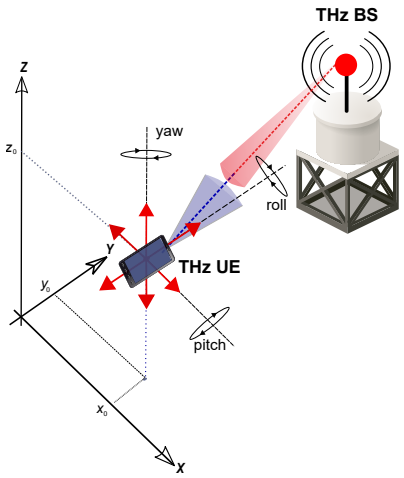

Fig. 1. The considered THz communications scenario.

a comprehensive measurement campaign characterizing user micromobility of different types of applications including FPT to circular boundary representing uninterrupted connectivity time interval;

- to facilitate modelling of THz cellular systems under micromobility impairments, we analyze the obtained measurement results and identify the critical statistical characteristics of micromobility patterns including distance-dependent velocity, drift to the origin, symmetricity with respect to the origin, and correlation between axes;
- to enable analytical and simulation studies of THz systems with micromobility, we develop the reference Markov models for all the considered applications and show that they serve as good approximations for applications that do not directly control user micromobility.

The rest of the paper is organized as follows. The equipment, considered applications, and the measurement methodology is described in Section II. We perform statistical data analysis of micromobility patterns of the considered applications in Section III. Detailed modelling insights are provided in Section IV, while the reference micromobility models are constructed and analyzed in Section V. Conclusions are drawn in the last section.

II. Measurement Methodology

This section is dedicated to the methodology of the performed measurements. We first introduce the system model and the conceptual approach. Then, we proceed with the description of the measurement equipment and selected applications utilized in experiments. Finally, we specify the data post-processing routines and define the metrics of interest.

A. System Model and Conceptual Approach

As the miniaturized equipment operating in the THz band with the intended antenna directivity still does not exist, the researchers are forced to perform indirect measurements reproducing the THz communications environment. With respect to micromobility measurements, the authors in [10] utilized the smartphone's embedded motion sensors to produce micromobility trajectories. However, this approach is inherently flawed as it is based on an inertial measurement system that is known to provide erroneous results. In this paper, we take a direct approach as described below.

We consider a point-to-point link between a stationary THz band base station (BS) and mobile UE as illustrated in Fig. 1. Both THz BS and UE are equipped with identical planar antenna arrays with $N_B \times N_B$ and $N_U \times N_U$ elements each. We assume a cone antenna radiation pattern [9], with non-zero gain over the main lobe of circular shape with the half-power beamwidth (HPBW) approximated by $102^\circ/N_B$ and $102^\circ/N_U$ [16]. In the considered system THz BS is assumed to be firmly fixed. Contrarily, THz UE is subject to micromobility affecting the beam searching process between UE and BS.

To be more specific, the micro-mobility in our system refers to small shakes and rotations of UE in hands of a user when he/she perceives a certain service. These impairments may affect communications even when a user is stationary. By utilizing geometric interpretation illustrated in Fig. 1 we observe, that the system enters the outage state when the centre of the UE beam leaves the circularly shaped area corresponding to HPBW of THz BS. It could happen due to small displacements of UE over x- and y-axes as well as due to yaw (vertical axis) and pitch (transverse axis) motions of UE in the user's hands. Observe that small displacements over z-axis as well as roll (longitudinal axis) motion do not severely affect the communications. The rationale is that these small-scale displacements are limited to just few tens of centimeters while the roll around the main axis does not change antenna alignment.

To capture UE micromobility it is sufficient to characterize the motion pattern of the centre of the UE beam. Instead of relying upon smartphone's motion sensors, we advocate for direct measurements of the motion patterns of imaginary UE beam. In this case, to track the location of the beam center we utilize a laser pointer firmly connected with the smartphone. The motion of the beam can thus be detected using either a light detection screen or a video camera. In this paper, we utilize the second approach.

B. Measurement Equipment and Setups

To facilitate our direct measurements campaign, illustrated in Fig. 2, we utilize a Nikon D3100 camera in the video recording mode at a resolution of 1280x720, 30 frames-per-second. A laser pointer with a beam diameter of 3 mm, an output power of 5 mW, and a light wavelength of 650$\pm$10 nm has been utilized. A tripod has been used to mount the camera capturing the motion of the laser pointer representing the centre of THz beam's HPBW. A laser pointer is firmly mounted on a mobile device and shines on the flat wall surface.

To improve contrast for further data processing the experiments have been carried out in a dark room. In our campaign, we target to capture micromobility patterns of four different applications. These are: (i) video viewing, (ii) phone calling, (iii) VR viewing, and (iv) racing game. As one may observe, the first three applications do not directly affect the UE micromobility pattern, while the latter one forces a user to perform semi-regular motions. In the video viewing

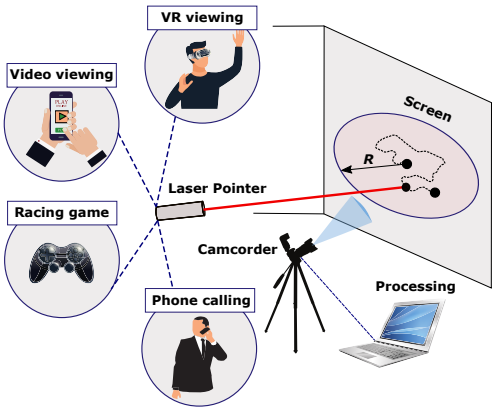

Fig. 2. The utilized measurement setup and environment.

application, the laser was attached to the back of the mobile phone, perpendicular to the horizontal axis of the mobile phone. Under the same conditions, experiments have been carried out for phone calling and racing game applications. For VR viewing applications, a laser pointer was also attached to the VR box console, so that the beam was parallel to the floor and shines on the wall. Owning to the restrictions of the measuring equipment and recalling that small angular speed may translate to relatively high linear speeds on the screen, we perform our experiments at 2 m separation distance from UE to the screen. Note that the absolute values, presented in this paper, need to be appropriately scaled up to operational distance between UE and THz BS. The observed area on the wall is 1.5×2.5 m.

For all the applications, a person was standing still and instructed to concentrate on the perceived content. In the case of racing game application, user was controlling a vehicle position on the road by utilizing built-in smartphone motion sensors. This resulted in semi-random movement patterns as a user progresses through the game. For video viewing application, a user was concentrated on watching a movie and the micromobility impairments are mostly due to the inability to hold UE in a completely stationary position. Note that a user was instructed to make no additional attempts to hold UE in a stationary position. For VR application, only one type of content has been considered – 3D movie. Here, the impairments are due to the non-stationary position of a user's head. Finally, for phone calling application, natural UE position close to the ear of a user was considered. For "smartphone" applications (video viewing, racing game, and phone calling) the results are reported further with respect to the "typical" orientation of the smartphone in the considered application, that is, the landscape for video viewing and racing game and portrait for phone calling.

To obtain the statistical data 10 independent experiments have been carried out for each considered application. The duration of each experiment has been set to 10 s. Once the experiment expires, the video is saved, and the experiment is repeated. The native camera resolution was 30 frames per second resulting in approximately 3300 sample points in the original trace for each application. To define the appropriate time resolution of the camera we need to account for the typical speed of UE movement in the hands of a user. In our experiments, we utilize a camera with an inherent time resolution is 1/30 s. The time resolution of one frame per 33 ms appears to be sufficient to capture the trajectory of a moving UE in hands of a user. Here, the critical thing is that in a single interval of 33 ms duration UE may not change direction of movement drastically. Thus, one can also interpolate the obtained data to the case of higher time resolution by using linear (or more complex) interpolation techniques.

C. Data Post-processing

To obtain the laser trajectory out of video recordings, the laser point is separated from the image using the background difference method [17]. Following this approach, by subtracting two adjacent frames and merging the resulting values in the range from 0 to 255, one obtains a background with zero pixel values, and non-zero pixels, where the laser is located. For a more accurate assessment of the position of the laser, not only adjacent frames are subtracted, but frames with a certain time step, so that the laser can change its position at a distance greater than the radius of the laser spot itself on the screen. To determine the centre of the laser spot, there is a pixel among those detected by the frame difference method, that has the highest non-zero value.

Note that sometimes, due to UE micromobility, a part of trajectory lies outside of the space captured by the camera, i.e., the visible camera frame. In this case, the trajectory is assumed to be bound to the captured frame boundary. Finally, to obtain traces with arbitrary time granularity, we have utilized the linear spatial interpolation method by determining coordinates of trajectory between the measured points.

D. Metrics of Interest

In practical applications, one of the main metrics of interest in the context of THz communications is how often outage happens and what are statistical characteristics of the time it takes for the system to go to the outage state. Note that the outage in wireless networks is a complex metric that depends on many system parameters, including not only distance but emitted power, antenna types (that affect antenna gains at both sides of a communications link, specific shapes of antenna radiation patterns, etc.), receiver sensitivity, cable losses, the set of modulation and coding schemes, etc. However, many of these parameters are not known at this stage of THz cellular systems development. Given the current information about measurements conditions reported in this section, the system parameters outlined above, and the statistical parameters reported in the paper, one can estimate the actual statistics by scaling the latter by utilizing simple geometry. As a result, in what follows, we investigate the statistical characteristics of the micromobility process with emphasis on FPT to the circular boundary based on the setup parameters reported in this section.

To facilitate mathematical or simulation based system-level analysis of THz networks under micromobility impairments

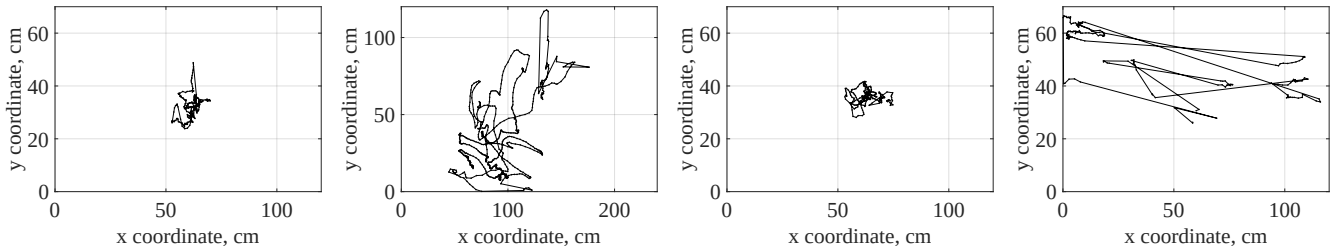

(a) Video viewing (b) VR viewing (c) Phone calling (d) Racing game

Fig. 3. Sample characteristic trajectories of the measured UE micromobility patterns for the considered applications.

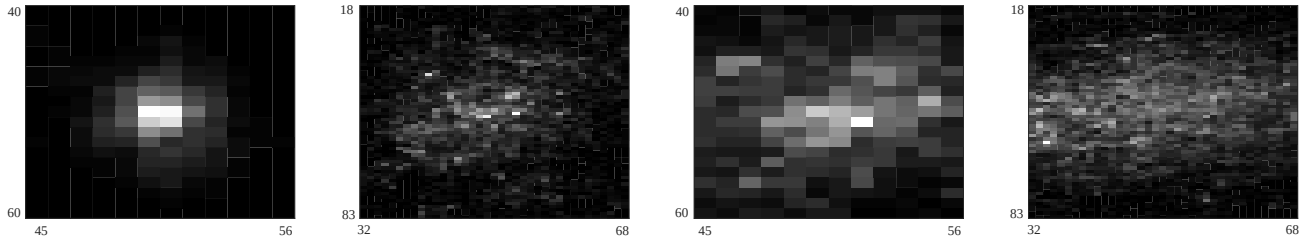

(a) Video viewing (b) VR viewing (c) Phone calling (d) Racing game

Fig. 4. Two-dimensional occupancy probability mass functions of the measured UE micromobility patterns for the considered applications.

one needs an accurate model. To construct such a model, an in-depth understanding of intermediate statistical characteristics is required. Thus, in this paper we also identify and analyze the critical statistical characteristics of micromobility patterns of the considered applications including distance-dependent velocity, drift to the origin, symmetricity with respect to the origin, and correlation between axes. Finally, based on the measured characteristics, we formalize reference Markov models for all the considered applications.

III. Statistical Data and Connectivity Time

In this section, we present our statistical analysis of the obtained micromobility patterns. We first concentrate on the first-order statistics and then proceed with characterization of uninterrupted connectivity time.

A. First-order Characteristics

Sample trajectories of UE mobility patterns are demonstrated in Fig. 3 for all the considered applications. The illustrated data allow us to make general conclusions about the basic characteristics of micromobility patterns. Analyzing the data presented in Fig. 3, one may confirm a common sense assumption that the most ”stable” application is video viewing, where the UE remains nearly stationary with only small micro displacements that happen randomly in up/down and left/right directions. The most ”unstable” application in terms of micromobility is racing game. Furthermore, the latter is also characterized by semi-deterministic behaviour with the motion to the left and right having much greater amplitude as compared to up and down shifts. VR viewing application is somewhat unique as its trajectory is characterized by much higher amplitude in all directions. Secondly, the trajectory of this application reminds paths of Brownian motion [18].

The two-dimensional occupancy probability mass functions (pmf) are presented in Fig. 4 for all the considered applications. To obtain these illustrations, the centre of the mass of the entire trajectory was taken as the centre of each experiment. The centres of different experiments were then aligned. The trajectory itself is linearly interpolated and sampled with a frequency of 100 points per second to increase the number of observations. The entire camera observation field is divided into 50 cells in horizontal and vertical directions leading to bin size of 3×5 cm. When the trajectory passes through these cells, the number of ”hits” is written. The number of observations falling into each cell is finally divided by the overall number of observations in a sample.

Analyzing the results in Fig. 4, one may conclude that there are no signs of radial symmetry in the considered data. This observation has crucial implications for the prospective modelling of UE micromobility patterns. In fact, to precisely capture UE micromobility one needs to use two-dimensional random processes that are characterized by much more complex methods required for their analysis in the context of THz communications. For example, the FPT characterizing the time to outage may not be available in closed-form for such processes. The data presented in Fig. 4 also confirm the conclusions made by utilizing sample paths with one noticeable exception. For phone calling and VR applications, the associated pmfs are much more dispersed as compared to video viewing application. The rationale is that in the latter one user puts his/her eye focus on the UE in hand while no such focus exists in phone calling. The same applies to VR viewing application, where a user is concentrated on the perceived content and is thus disoriented in space. The extreme variance observed for racing game is due to the application itself forcing the user to make left/right motions with UE, which are visible in both Fig. 3 and Fig. 4.

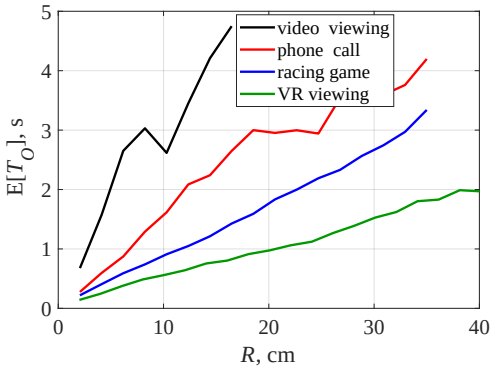

(a) Mean value

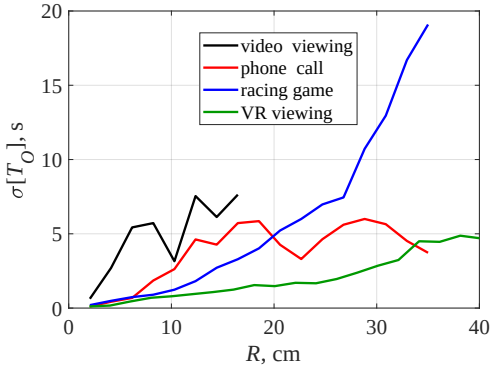

(b) Standard deviation

Fig. 5. FPT to circular boundary for the considered applications.

The presented data allow making a number of hypotheses critical for modelling of UE micromobility patterns. First of all, all the considered applications might be characterized by drift to the origin of different orders of magnitude. Furthermore, there might be symmetry in motion with respect to the origin at least for some applications. We test these and also other less evident hypotheses further in Section IV, where we study complex statistical micromobility properties of applications.

B. Time to Outage Characterization

Before we proceed with the modelling insights, we first bring readers' attention to the critical metric of interest with respect to THz communications – time to an outage for the considered applications. For illustration purposes we consider a simple cone antenna model implying that the boundary of interest is the circle with the centre at the initial point. Note that in what follows, we assume that the beam searching procedure is perfect, i.e., every time when beam searching is performed, UE and BS beams are perfectly aligned.

Observe that according to the straightforward approach one may only obtain a single FPT observation from a single experiment following the following assumption: at the beginning of the experiment, the connection is established, i.e., the radiation patterns of THz BS and UE are perfectly aligned with each other with centres of HPBWs lying on the same axis. FPT occurs once per experiment if, due to micromobility, the beam goes beyond a circle with a certain radius specified by THz BS antenna HPBW. However, to increase the number of FPT observations and obtain reliable statistics, we assume that once antennas misalignment occurs, beam searching is performed to align them back. Following this approach, the number of FPT observations in a single experiment of 10 s duration can be greater than one. To remove residual correlation in the micromobility pattern we also skip exactly 1 s from the time instant when beam misalignment is recorded.

To be more specific, at the time instant $t = 0$ we start to track first FPT value. Once the trajectory reaches the boundary, we store this first FPT value, skip 1 s and start tracking the second value. Here, 1 s is utilized to get rid of residual serial correlation in FPT values. The choice of exactly 1 s was a compromise between the number of samples in the FPT trace we can obtain (the higher the value the smaller the number of observations) and the effect of residual dependence. The latter was assessed by constructing a normalized autocorrelation function (NACF) for original mobility patterns. For all the applications, except for "racing game" the value of 1 s provides the compromise between the amount of serial correlation in the data and the sample size. The case of "racing game" is very specific due to semi-random patterns with explicit left-right movements induced by the application itself. Here, we observed that correlation lasts much longer than 1 s but we still utilized 1 s as the time interval to be able to have a sufficient number of observations in the FPT trace.

Note, that the serial correlation does not affect point estimates of mean values. On the other hand, it may severely bias the variance and standard deviation and drastically deteriorate confidence limits. At the same time, the width of the confidence limits is also affected by the sample size. Thus, there is a trade-off between the sample size and the accuracy of confidence limits. For this reason, in what follows, we utilize point estimates only that are not affected by this trade-off. Note that the values of standard deviations illustrated below for several metrics of interest can also be attributed to both specific properties of random walks often characterized by high variability and the effects of residual correlation.

Analyzing the results presented in Fig. 5 one may observe that, expectedly, the mean FPT increases as the radius gets larger, i.e., antenna with fewer number of elements is utilized or distance between THz BS and UE is increased. The shortest time, on average, is observed for VR viewing application

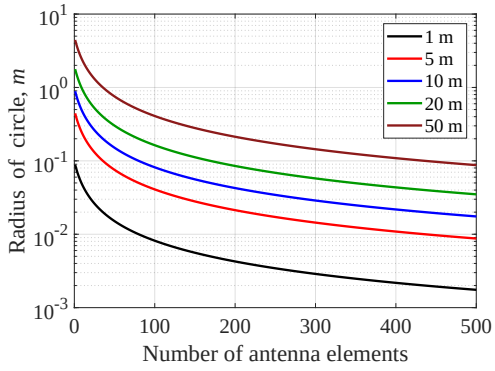

Fig. 6. HPBW radius as a function of the number of antenna elements.

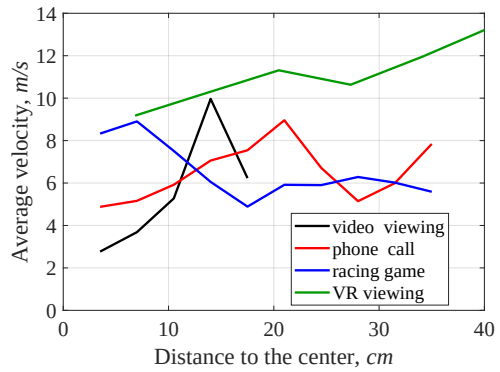

(a) Mean value

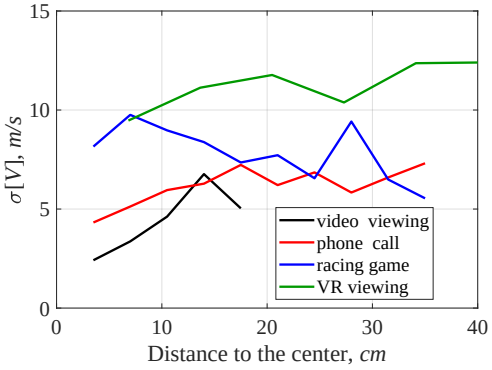

(b) Standard deviation

Fig. 7. Distance-dependent velocity characteristics.

while the longest time – for video viewing application. We would like to specifically note that for the latter application no passage times have been observed for radii higher than 18 cm. To complement these data, in Fig. 6 we also provide the radius of the HPBW projection at the plane orthogonal to the line-of-sight (LoS) path between the THz BS and UE, where HPBW is estimated as $102^\circ/N_B$, while the radius is found by using conventional geometry.

IV. Micromobility Modeling Insights

As we observed, UE micromobility patterns heavily depend on the type of applications in use. Moreover, as demonstrated in [11], characteristics of the random process describing the mobility pattern may affect design choice for THz communication systems, i.e., the type and parameters of the beam searching process. Thus, we now proceed by revealing the major properties critical for micromobility modelling. Particularly, we characterize distance-dependent velocity and drift to the origin of the considered applications as well as test dependence between mobility processes over x- and y-axes and symmetry with respect to the origin. These properties provide detailed insights into the modelling of considered UE micromobility patterns.

A. Distance-dependent Velocity

One of the major factors affecting the intensity of outages caused by micromobility is the velocity of the micromobility process. To this aim, Fig. 7 illustrates the distance-dependent velocity characteristics including the mean and standard deviation for all the considered applications. These statistics have been calculated as follows. For each application we divide the maximum observed distance to the center into $N = 10$ values: $(x_0, x_1), (x_2, x_3), .., (x_{2N-1}, x_{2N})$. Next, we go through all the trajectories and estimate the length of the traversed path Δs. The latter is set to $\Delta t = 1/100$ s. For each defined range we then convert them to the velocity by estimating $v = \Delta s/\Delta t$. Finally, we average all velocity observations falling into the same range (x_{i-1}, x_i).

Analyzing the results presented in Fig. 7, one may observe that for all the considered applications but racing game, the mean velocity tends to increase as a function of the distance from the centre. Furthermore, as distance increases standard deviation increases as well. The behaviour of the racing game application is explained by a unique type of mobility heavily affected by the left and right movements. Recall that the velocity metric is scalar in nature. Thus, the considered behaviour of the mean velocity metric increasing with the radial distance from the origin and visual observation of sample paths and pmfs in Fig. 3 and Fig. 4 may imply that the micromobility processes may have a non-zero drift to the origin. We now proceed with assessing this metric.

B. Radial Drift To the Origin

One of the useful properties of analytically tractable stochastic processes is the independence of increments. For example, the UE micromobility model utilized by the authors in [11] assumes unbiased random walk in two dimensions that are known to return to the centre with a probability less than one, i.e., it may never return to the position it originally started at. When the user is in a stationary position one may not expect permanent changes in the location of the beam centre. From the practical perspective, it would imply that outages caused by micromobility will happen much less frequently as compared to unbiased mobility. Thus, having revealed distance dependent velocity characteristics we now proceed with the distance-dependent drift to the origin characterization.

Fig. 8 demonstrates drift to the origin for all the considered applications. Note that there are a number of ways to define the drift. Here, we define drift as the conditional probability of moving towards the origin and derive it as follows. We first divide the maximum distance from the centre to

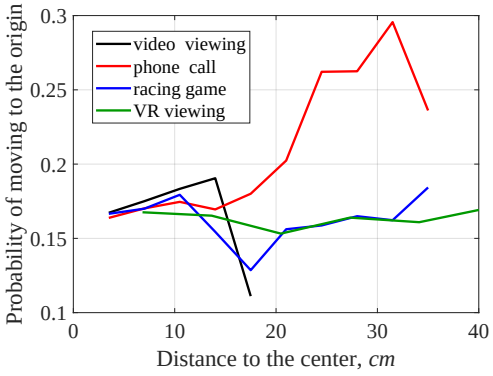

Fig. 8. Distance-dependent radial drift to the origin.

TABLE I
RESULTS OF THE KOLMOGOROV-SMIRNOV TEST FOR SYMMETRY

	p-val.	statistic	p-val.	statistic	p-val.	statistic
Sign. level	0.01		0.05		0.1	
Video viewing	0.073	0.171	0.060	0.171	0.055	0.171
Phone call	0.056	0.068	0.047	0.068	0.042	0.068
Racing game	0.018	0.166	0.015	0.166	0.013	0.166
VR viewing	0.026	0.179	0.022	0.179	0.02	0.179

N non-overlapping ranges. Then, for each trajectory point falling into a given range we determine the direction of the next movement. The overall drift corresponding to the range (x_{i-1}, x_i) is obtained by dividing movements to the centre by the overall number of movements within this range. After accumulating statistics for all experiments for a given application, the average drift value is calculated.

Discussing the results presented in Fig. 8, one may notice that all applications are characterized by non-negligible drift to the origin. The difference in the absolute value of the drift at a certain distance to the centre can be attributed to the differences in the amplitude of the micromobility associated with a given application. Still for three the considered applications, VR viewing, video viewing, and racing game the drift remains almost intact with the distance. For phone calling, however, the trend towards the centre drastically increases with the distance from the origin. Thus, the models utilized for capturing mobility patterns of realistic applications in THz communications have to incorporate drift to the origin.

C. Symmetry of User Micromobility

One of the ways to simplify the modelling of UE micromobility patterns is to reduce the dimension of the process. Particularly, if there is a radial symmetry in the micromobility characteristics it would imply that one may reduce its characterization to a one-dimensional random walk. We now proceed to study symmetry in the UE micromobility.

The conclusion on symmetry can be assessed by: (i) visual observation of traces and (ii) comparison of the statistical properties of UE mobility patterns in, e.g., Cartesian quadrants. In the latter case, the necessary condition on statistical symmetry can be provided by comparing two-dimensional pmfs associated with each quadrant of Cartesian coordinate axes. In what follows, to assess the symmetry, the Kolmogorov-Smirnov test was applied [19] to assess the match of the distributions from different quadrants.

As we have observed analyzing the two-dimensional pmfs presented previously in Fig. 4, none of the processes associated with the considered applications should pose symmetrical properties with respect to the origin. One exception is the video viewing application that is characterized by relatively uniform spread around the origin. The results of the distribution comparison by using Kolmogorov-Smirnov statistical test for first and third quadrants are shown in Table I for significance level, α, set to 0.01, 0.05 and 0.1. Note that different p-values are attributed to slightly different samples sizes. As one may observe, out of all the considered applications, none is reliably characterized by symmetry. Similar conclusions have been made for other pairs of quadrants.

The presented results imply that to capture the considered stochastic patterns one has to explicitly capture motions in a different direction that may require utilization of two-dimensional processes. This is especially true for applications forcing users to behave in a non-symmetric way, e.g., the considered racing game. For the rest of the applications, one may still try to utilize one-dimensional approximations to get basic approximations of UE mobility patterns.

D. Dependence and Correlation

Another way to simplify the modelling of the UE micromobility process is to assume that mobilities over x- and y-axes are independent of each other. For example, this hypothesis has also been taken in [11] without any proofs. To prove that motions along x- and y-axes are independent, it is sufficient to prove that individual increments are independent.

We start assessing the correlation between increments of individual processes. The initial data for the test have been obtained using the following procedure. First, we utilize traces to obtain values of Δx and Δy increments corresponding to successive time increments Δt. Then, we estimate the correlation coefficient as follows

$$\hat{r} = \frac{\sum(\Delta x - \overline{\Delta x})(\Delta y - \overline{\Delta y})}{\sqrt{\sum(\Delta x - \overline{\Delta x})^2 \sum(\Delta y - \overline{\Delta y})^2}}, \quad (1)$$

where $\overline{\Delta x}$ and $\overline{\Delta y}$ are the corresponding mean values.

The coefficient of correlation between absolute displacements along x- and y-axes for all the considered applications is illustrated in Fig. 9 as a function of the increment size along with the confidence intervals estimated according to the "rule-of-thumb", $\pm 2/\sqrt{N}$, where N is the number of measurements available [20]. As one may observe analyzing the presented data, although there are non-negligible correlations between absolute values of increments along x- and y-axis, for three of the considered four applications, VR viewing, video viewing, and phone calling, the dependence is rather weak as the correlation values are close to zero. The fourth considered application, racing game, is characterized by a much higher correlation coefficient reaching the value of -0.4 starting from Δt of approximately 0.2. The explanation is related to the very specific mobility pattern of this application, see Fig. 3(d), with evident semi-random oscillations along the x-axis.

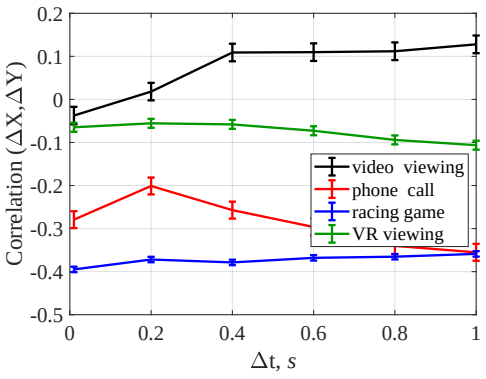

Fig. 9. Correlation between increments over x- and y-axes.

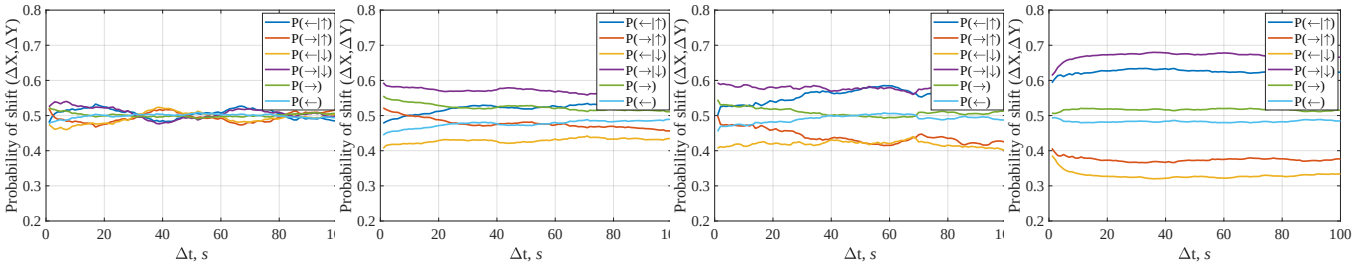

(a) Video viewing (b) VR viewing (c) Phone calling (d) Racing game

Fig. 10. Conditional and unconditional probability plots.

Recall that the correlation coefficient in (1) captures only the tendency to linear dependence between analyzed components. To assess independence between x- and y-axes increments for applications having negligible correlation, further analysis is required. We perform this in Fig. 10 by comparing the probabilities of left/right displacement along x-axis conditioned of the event of up/down movement along y-axis, $P(\leftarrow \mid \uparrow)$, $P(\leftarrow \mid \downarrow)$, $P(\rightarrow \mid \uparrow)$, and $P(\rightarrow \mid \downarrow)$, with respective unconditional probabilities, $P(\leftarrow)$ and $P(\rightarrow)$, as a function of the time interval Δt. Note that compared to the correlation coefficient, conditional probabilities capture all types of dependencies between components.

Analyzing the data presented in Fig. 10, one may first notice, that for racing game the correlation revealed in Fig. 9, translates directly to drastically different values of conditional and unconditional probabilities. Particularly, $P(\leftarrow \mid \uparrow)$ is higher than 0.6 while $P(\leftarrow \mid \downarrow)$ is lower than 0.4 for all Δt. At the same time, the unconditional probability $P(\leftarrow)$ is around 0.5 for all considered values of Δt. For the rest of the considered applications, the differences are much smaller. Particularly, for video viewing these probabilities almost coincide across the whole considered range of Δt values. The values of conditional and unconditional probabilities are also close for VR viewing and phone calling applications.

The presented results imply that the dependence between mobility over x- and y-axes are not critical for applications having no specific mobility pattern induced by the type of application. Thus, to simplify the modelling procedure one may attempt to capture the movement along axes by using independent random walks. To facilitate this approach in Fig. 11 and Fig. 12 we present distance-dependent velocity and drift to the origin characteristics. Analyzing these illustrations, one

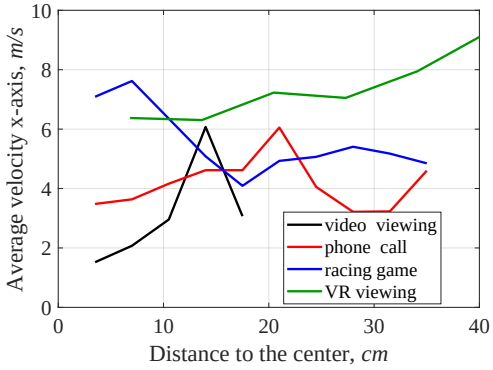

(a) X-axis mean value

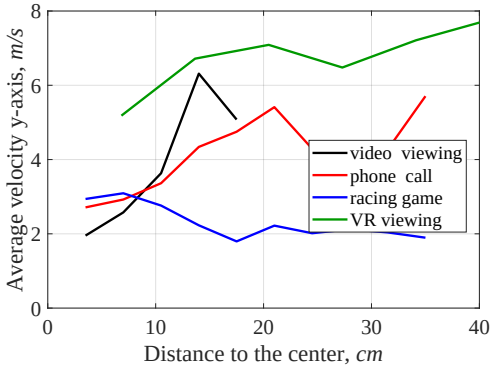

(b) Y-axis mean value

Fig. 11. Distance-dependent velocity characteristics over x- and y-axes.

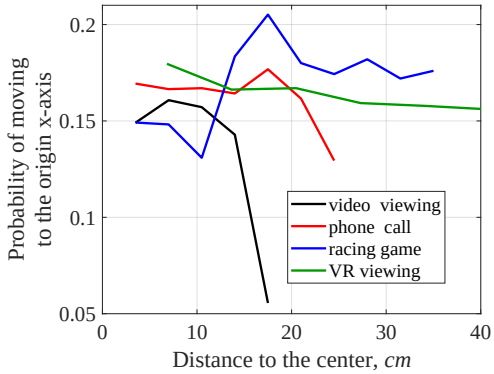

(a) Drift to the origin over the x-axis

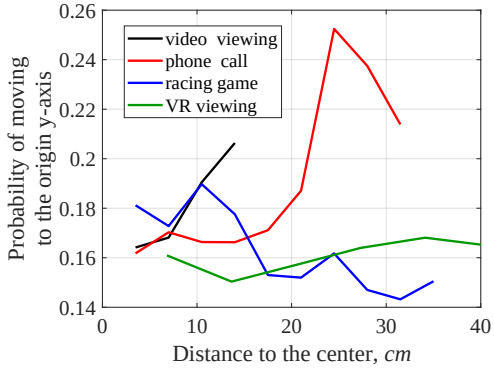

(b) Drift to the origin over the y-axis

Fig. 12. Distance-dependent drift to the origin over x- and y-axes.

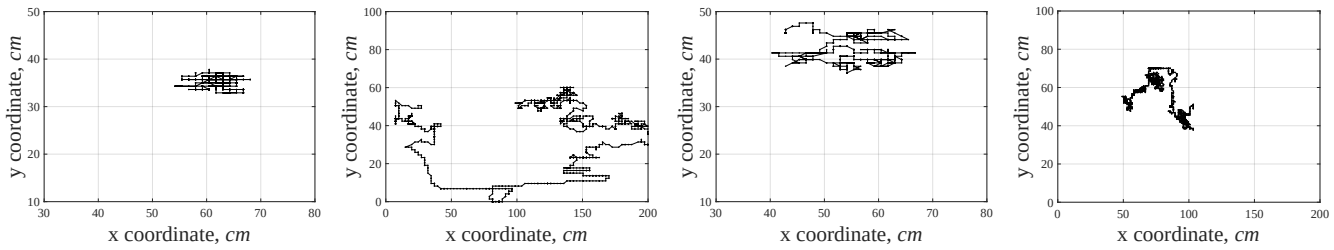

(a) Video viewing (b) VR viewing (c) Phone calling (d) Racing game

Fig. 13. Sample paths of simulated micromobility trajectories for the considered applications.

may not only deduce quantitative characteristics but observe that, for example, for video viewing, VR viewing, and phone calling applications the velocity values over x- and y-axes almost closely resemble those of two-dimensional mobility. For racing game application the absolute values are drastically different due to the nature of the mobility pattern. Completely different results are, however, observed by comparing the drift to the origin of two-dimensional mobility pattern and decomposed x- and y-axes patterns. For example, for phone calling application one may observe, that the trends over x- and y-axes are mirrored, while for VR viewing application they remain constant for both axes resembling the behaviour of the two-dimensional mobility pattern. Finally, we note that for those applications, inducing specific semi-regular mobility patterns, e.g., racing game that forces the user to perform semi-random oscillations, explicit two-dimensional models with distance-dependent velocity and drift from the centre are required.

V. Reference Models

The UE micromobility of different applications may provide significant performance degradation for THz communications. The prospective analysis and optimization of THz communications systems under micromobility impairments can be performed by utilizing system level simulations or mathematical analysis. To facilitate both types of analyses, in this section, we specify the reference Markov-based UE micromobility models for the considered applications. We then proceed by comparing their performance in terms of first- and second-order properties including FPT to the circular boundary characterizing the time the link is active. Finally, we presents the results of simplified decomposed models, where x-axis and y-axis mobilities are represented by independent processes.

A. Direct Markov Modeling

In order to parameterize the Markov model, we need to determine the number of states, $N \times N$, corresponding to the screen grid size, and estimate the transition probabilities p_{ij}, $i, j = 1, 2, \ldots, N^2$. There is a number of generic fitting algorithms developed for Markov models, such as those based on the expectation-minimization (EM) technique [21] or adaptation of maximum likelihood estimation [22]. However, these techniques are useful only when the internal structure is not clearly observable or the number of states cannot be deduced from physical parameters.

Before we proceed with an estimation of transition probabilities, there are two critical parameters to determine. These are the time and spatial resolutions of the model, Δs and Δt. Note that in spite of the feasibility to operate with any time resolution by utilizing the interpolation techniques, to avoid additional errors we utilize the native resolution of $1/30$ s. The choice of the spatial resolution Δs, implicitly defining the number of states of the chain, N^2, is a question of the trade-off between the sample size and the capability of the model to accurately predict the main metric of interest – FPT. For the latter to be feasible, Δs has to be at least five times smaller than the considered HPBW radius [23], [24]. By recalling HPBW approximation by $102^\circ/N$, where N is the number of antenna elements forming directional radiation pattern in appropriate plane, for typical THz communication distances (up to 50-100 m) and modern antenna arrays (at least, 32×32 antenna elements) one is mainly interested in radii of at least few centimetres. On the other hand, increasing the spatial resolution decreases the sample size to parameterize the model. Thus, in what follows we will utilize two values of Δs set to 2.5 and 1.25 cm corresponding to $N^2 = 2500$ and $N^2 = 10^4$, respectively.

Once the number of states is selected, we proceed to determine the transition probabilities p_{ij}, $i, j = 1, 2, \ldots, N^2$ by using the conventional statistical methodology. We first define the state boundaries between the states and then calculate the number of state changes for the particular values of i and j between the previous and the current values in the trace and divide it by the number of samples in the trace. Then, these probabilities are organized in the transition probability matrix. The dimension of such a matrix corresponds to the square of the grid dimension, i.e., for example, if the quantization grid is $N \times N$, then the matrix of transition probabilities is $N^2 \times N^2$. To save memory, a list of nonzero transition probabilities is used to store transition probability matrices.

B. Accuracy Assessment

To assess the accuracy of the proposed Markov model we concentrate on two characteristics, two-dimensional pmf of the micromobility process and mean FPT. Note that the former is an intermediate characteristic allowing to access the suitability of the proposed class of models, while the final judgement on the accuracy should always be based on the FPT metric. The simulation of the Markov model is initiated from the starting point of experiments. Then, given a randomly generated number uniformly distributed in (0,1), the next cell is determined by using the transition probability matrix.

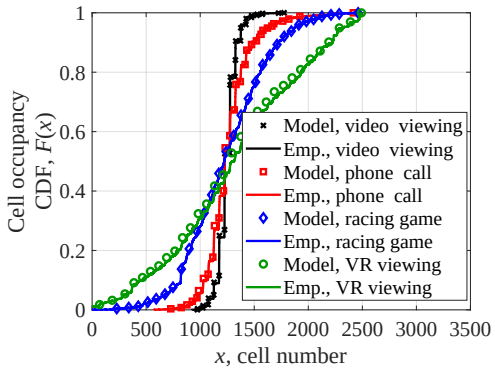

(a) Grid 50×50, Δt=1/30

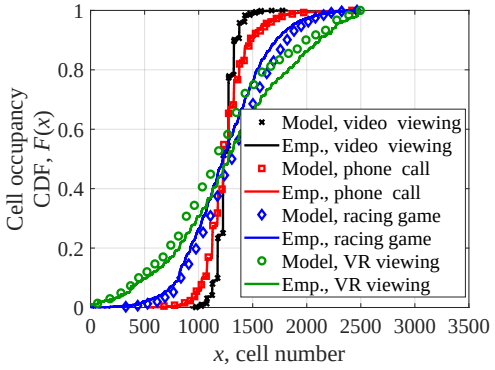

(b) Grid 50×50, Δt=1/100

Fig. 14. Empirical and modeled two-dimensional occupancy CDFs.

The sample trajectories of the model are illustrated in Fig. 13 for grid size 50×50 and native time resolution of $\Delta t = 1/30$ s. By comparing the presented data with those shown in Fig. 3 we observe, that for all applications but racing game, all the inherent properties are preserved. Particularly, the range of trajectories for video viewing and phone calling applications is limited and comparable to each other while the range for VR viewing is significantly higher requiring a large grid for visual representation. However, in the case of racing game application, one does not observe an intrinsic pattern dominated by left/right movements enforced by the game.

We now proceed with Fig. 14 illustrating cell occupancy cumulative distribution functions (CDF) obtained using the empirical and modeled data for grid size 50×50 and time resolution of $\Delta t = 1/30$ and $\Delta t = 1/100$. For clarity of comparison, we utilize exactly the same sample size for the modelled data as in real experiments (approximately 3300 observations at a native time resolution of $\Delta t = 1/30$ s and 10^4 observations for $\Delta t = 1/100$ s). Here, instead of utilizing two-dimensional CDF, we enumerate all the cells and represent CDF in a conventional one-dimensional form convenient for visual assessment. As one may observe, for all the considered applications, CDFs of the model approximate those of empirical data very well. However, the applications having the smallest range of values, video viewing and phone calling, are characterized by better approximation. The worst approximation is observed for racing game application that is known to pose significant correlational properties.

TABLE II
KOLMOGOROV-SMIRNOV TEST FOR TWO-DIMENSIONAL CDFS (α = 0.1)

Size grid	Δt	Video viewing	Phone calling	VR viewing	Racing game
50×50	1/30	Y	Y	N	N
	1/100	Y	N	N	N
100×100	1/30	N	N	N	N
	1/100	N	N	N	N

We complement the visual test by the Kolmogorov-Smirnov one whose results are reported in Table II for the level of significance set to $\alpha = 0.1$, two considered grids, 50×50 and 100×100, and two time steps, $1/30$ and $1/100$. Note that Y (Yes) and N (No) refer to passing and not passing the statistical test, respectively. As one may deduce analyzing the presented data, video viewing and phone calling applications pass the test while the other two applications fail it. However, we specifically note that the Kolmogorov-Smirnov test is one of the strongest distributional tests [25].

We now proceed with assessing the accuracy of the FTP approximation. To this end, Fig. 15 presents mean FPT values obtained using the empirical and modelled data as a function of the HPBW radius for a grid size 50×50 and time resolution of $1/30$. As one observes, for all the considered applications but for the racing game, the mean FPT is well captured to the radius of approximately $10-15$ cm. Recalling the data in Fig. 6, we see that these radii are well in line with the prospective THz equipment that is expected to feature hundreds of antenna elements at maximum distances of up to 50 m [9]. Thus, for these applications, the developed Markov models may serve as reliable approximations.

Analyzing the data presented in Fig. 15 further, one may notice that starting from around $10 - 15$ cm the model data start to overestimate the actual mean FPT for the considered applications. For the gaming application, the difference is evident even at small values. There are plausible explanations behind this behaviour that may both be attributed to the inherent properties of the utilized class of stochastic processes – Markov processes. Recalling the exposure in [23], [26] the generic structure of FPT distribution inherent for random walks of any dimension is a mixture of exponential and power-law components, i.e., $Ct^{-\alpha D}e^{-\beta t}$, $t \geq 0$, where $\alpha > 0$, $\beta > 0$, $C > 0$ are some constants, $D > 0$ is a drift coefficient. The exponential part is inherent for short-term memory processes such as the Markov process utilized in our study, while the power-law is induced by long-term memory, e.g., large-scale dependence [27]. The impact of the latter is partially compensated by the drift coefficient. Thus, the processes characterized by long-term correlational properties are mainly affected by the second term contradicting the implicit Markov assumption. Recalling the data presented in Subsection IV-D, in the case of racing game the memory is much longer compared to the one-step assumption of Markov modelling putting more weight on the power-law behaviour of CDF. We speculate that this might be the case for any application that controls user behaviour,

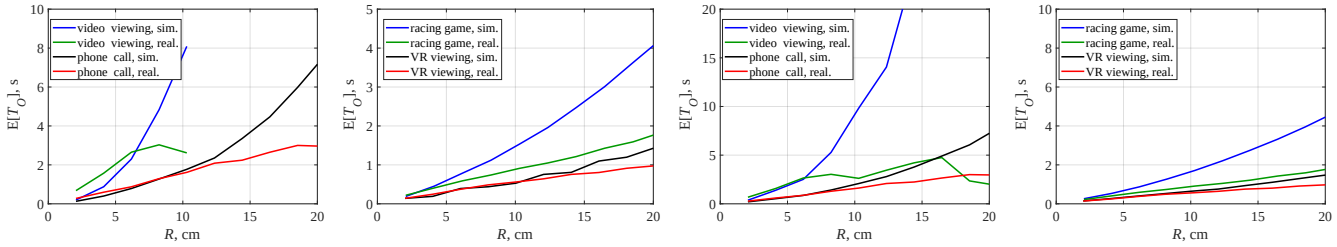

(a) Grid 50×50 (b) Grid 50×50 (c) Grid 100×100 (d) Grid 100×100

Fig. 15. Empirical and modeled mean FPTs to the circular boundary.

i.e., games utilizing gyroscope and accelerometer. Finally, the divergence of modelled FPT from empirical one can also be partly attributed to insufficient data available for larger radii.

To get further insights, for two applications, whose models pass the Kolmogorov-Smirnov test for two-dimensional occupancy CDFs, video viewing and phone calling, we demonstrate empirical and modeled FPT CDFs in Fig. 16 for several radii. As one may observe, for both small and large radii, e.g., < 4 cm and > 10 cm, CDFs do not coincide with each other. However, for moderate radii of around 4-8 cm, there is a good match between them. The rationale is that small considered values of radii are comparable with the grid size (2.5 cm and 1.25 cm for considered 50×50 and 100×100 grids). The observed deviations are caused by the choice of the initial cell in the centre of the grid, which is selected randomly out of 4 cells located in the centre. Increasing the radius leads to a very good match between CDFs while even further increase again results in the mismatch. These latter deviations might be explained by an insufficient amount of observations available for analysis, especially, in the case of video viewing application.

The abovementioned observations are also confirmed in Table III showing the results of the Kolmogorov-Smirnov test for video viewing and phone calling applications. As one may observe, both applications do not pass the test up until 6 cm for video viewing and 8 cm for phone calling applications. Then, the test confirms that the models correctly predict the empirical data up until the point where the number of observations becomes too small to build CDF reliably. As a result, we may conclude that for applications, where there is no explicit control of user behaviour, the developed Markov models provide a good approximation of empirical data.

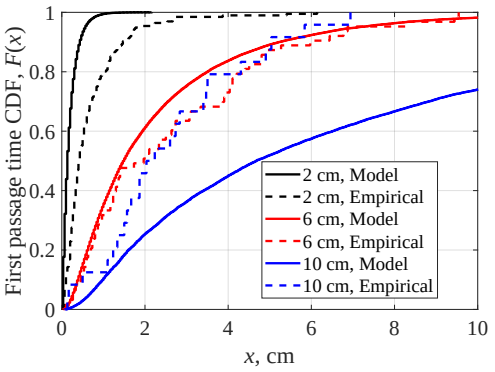

(a) Video viewing

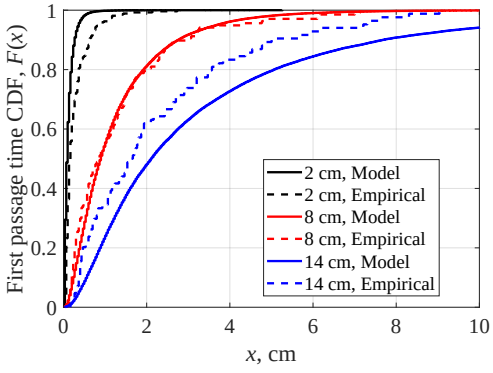

(b) Phone calling

Fig. 16. Empirical and modeled FPT CDFs.

C. Simplified Models

In the previous sections, we revealed that the micromobility patterns of real applications have very specific properties (dependence between axes, drift to the origin, distance-dependent velocity, etc.) that prevents from applying simple modelling techniques based on decomposition principles, e.g., by utilizing independent Brownian motions for individual axes as it is done in [11]. Furthermore, the models we provided in Section V.A are not analytically tractable due to extreme state-space, e.g., using 2500 and 10^4 as the number of states. These models can be utilized for benchmarking purposes when developing new analytically tractable models for UE micromobility.

In an attempt to define an analytically tractable model for link-level performance assessment of THz systems according to the methodology reported in [11], in addition to the two-dimensional reference model reported in the previous section, we also define models that might potentially have analytical properties including: (i) decomposed Brownian motion model with independent movements along x- and y-axes, where we drop potential dependence between axes movements as well as a drift to the origin and distance-dependent velocity,

TABLE III
KOLMOGOROV-SMIRNOV TEST FOR FPT CDFS, $\alpha = 0.1$

Radii, cm	2	4	6	8	10	12	14	16
Video viewing	N	N	Y	Y	N	N	N	N
Phone calling	N	N	N	Y	Y	Y	N	N

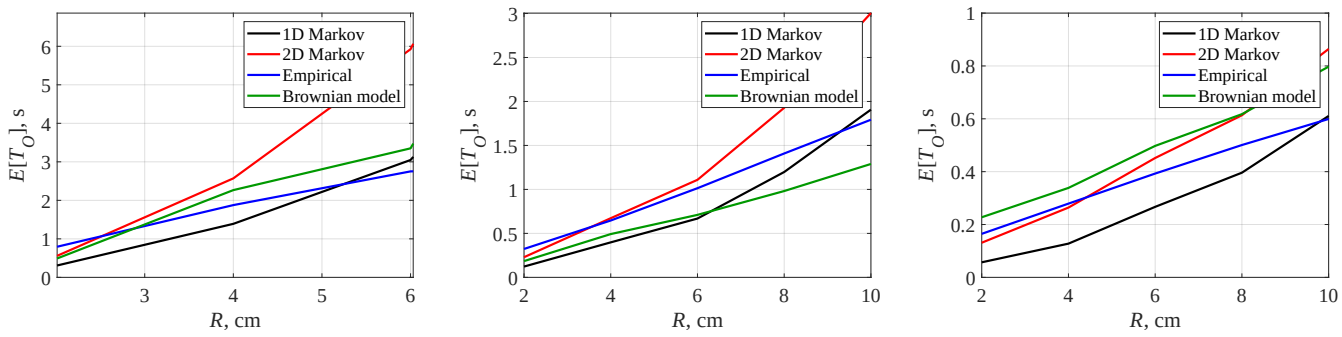

(a) Video viewing (b) Phone calling (c) VR viewing

Fig. 17. Illustration of empirical and modeled mean FPT values for three considered applications.

TABLE IV
SUMMARY OF MICROMOBILITY CHARACTERISTICS AND MODELING INSIGHTS

Characteristics	Video viewing	Phone calling	VR viewing	Racing game
Radial symmetry	Yes	No	No	No
Velocity as a function of distance	Increases, $3-10$ m/s	Constant, 7 m/s	Increases, $9-13$ m/s	Decreases, $9-5$ m/s
Drift to the origin as a function of distance	Decreases, $0.17-0.11$	Increases, $0.17-0.3$	Constant, 0.17	Constant, 0.17
Axes dependence	Negligible	Moderate	Negligible	Strong
Axes increment correlation coefficient	0.0	-0.2	0.0	-0.4
X-axis velocity as a function of distance	Increases, $1-6$ m/s	Increases, $3-6$ m/s	Increases, $6-9$ m/s	Decreases, $7-4$ m/s
Y-axis velocity as a function of distance	Increases, $2-8$ m/s	Increases, $3-5$ m/s	Increases, $5-8$ m/s	Decreases, $3-2$ m/s
X-axis drift as a function of distance	Decreases, $0.17-0.05$	Decreases, $0.17-0.13$	Constant, 0.17	Increases, $0.13-0.21$
Y-axis drift as a function of distance	Increases, $0.17-0.21$	Increases, $0.17-0.25$	Constant, 0.17	Decreases, $0.19-0.14$
Markov modeling	Yes	Yes	Limited	No

and (ii) decomposed one-dimensional Markov models with independent movements along x- and y-axes, but accounting for the distance-dependent velocities and the drift to the origin. The results in terms of the mean FPT are illustrated in Fig. 17. Note that here we intentionally omit racing game application as it is characterized by different semi-regular nature and thus require different modelling methods. Expectedly, the best approximation is observed for the two-dimensional Markov model as it captures all the statistical characteristics of the considered mobility patterns. The rest of the models, however, provide a rather inaccurate approximation of realistic patterns. Furthermore, the simplest fully independent and unbiased Brownian motion model performs comparably to the one-dimensional Markov model, where both distance-dependent velocity as well as a drift to the origin are taken into account.

VI. CONCLUSIONS

To facilitate the development of THz beam searching algorithms, in this paper, we comprehensively characterized the UE micromobility process for different applications. We considered state-of-the-art applications including video viewing and VR viewing, phone calling and racing game and characterized first- and second-order statistical properties such as sample trajectories, two-dimensional occupancy distributions and FPTs. The latter is of critical importance as it characterizes the time to an outage in THz communications systems.

Having set the aim for stochastic mathematical modelling of UE micromobility process we also revealed modelling implications of UE micromobility patterns of the considered applications. We have shown that none of those is characterized by radial symmetry. Furthermore, the velocity and drift of the random mobility patterns are both distance-dependent in nature. Thus, to accurately capture stochastic properties of UE micromobility patterns, these properties call for complex modelling approaches involving two-dimensional random walks with non-independent increments. The summary of statistical characteristics and modelling insights is presented in Table IV.

We also developed reference two-dimensional Markov models and demonstrated that they are only suitable for applications with low and purely random dynamics such as video viewing and phone calling. We also note that the Markov models considered in this paper are not suitable for the case when the application directly controls user behaviour as in the case of “race gaming”. Here, one needs to utilize mobility models characterized by long correlation resulting in visible “flights” superimposed with local fluctuations. The models suitable for capturing such patterns are Levy flight and Brownian motion with jumps [18]. Thus, one of the major conclusions of the paper is the ”call for accurate and analytically tractable UE micro-mobility models” for link-level performance assessment of THz systems according to the methodology reported in [11], and based on the measurements campaign and statistical analysis of UE micromobility patterns provided in this paper. Finally, we emphasize that the actual micromobility pattern may not consist of a single application as users may change them on-the-fly or, for example, occasionally change smartphone orientation. These complex patterns can be modelled as a superposition of the considered applications superimposed with occasional outliers.

The statistical analysis reported in this paper can be useful

for the design of beam searching schemes for THz systems that tries to avoid outages caused by micromobility or at least alleviate the effect of outages. There are two potential designs for such systems: (i) initiate beam searching when the connection is lost, so-called, WLAN design and (ii) initiate beam searching regularly as it is done in, e.g., 5G New Radio (NR) systems. For the latter case, the beam searching is performed in each frame of 10 ms in duration which is significantly smaller than the average FPT time reported in this paper. However, it is only feasible in NR as the utilized antennas arrays are rather limited in terms of the number of elements, e.g., arrays 16×4, 32×4 are planned to be utilized for mmWave NR. When the number of antenna elements will increase to, e.g., 128×128 or even higher which is needed in THz systems to compensate for two orders of magnitude increase in the path loss, the time required for beam searching can be extremely high preventing the regular beam searching design as in NR systems. Note that the use of hierarchical beam searching also will greatly reduce the coverage of prospective THz BS and may not be even feasible at all for THz arrays having a high number of elements forming directional radiation patterns. As a result, for efficient use of THz systems both drastic improvements in algorithmic beam searching design and a further significant reduction in the array switching time are needed.

REFERENCES

[1] M. Polese, J. Jornet, T. Melodia, and M. Zorzi, "Toward end-to-end, full-stack 6G terahertz networks," *arXiv preprint arXiv:2005.07989*, 2020.

[2] V. Petrov, J. Kokkoniemi, D. Moltchanov, J. Lehtomaki, Y. Koucheryavy, and M. Juntti, "Last meter indoor terahertz wireless access: Performance insights and implementation roadmap," *IEEE Communications Magazine*, vol. 56, no. 6, pp. 158–165, 2018.

[3] T. S. Rappaport, Y. Xing, O. Kanhere, S. Ju, A. Madanayake, S. Mandal, A. Alkhateeb, and G. C. Trichopoulos, "Wireless communications and applications above 100 GHz: Opportunities and challenges for 6G and beyond," *IEEE Access*, vol. 7, pp. 78729–78757, 2019.

[4] V. Petrov, G. Fodor, J. Kokkoniemi, D. Moltchanov, J. Lehtomaki, S. Andreev, Y. Koucheryavy, M. Juntti, and M. Valkama, "On unified vehicular communications and radar sensing in millimeter-wave and low terahertz bands," *IEEE Wireless Communications*, vol. 26, no. 3, pp. 146–153, 2019.

[5] J. M. Jornet and I. F. Akyildiz, "Channel capacity of electromagnetic nanonetworks in the terahertz band," in *2010 IEEE International Conference on Communications*, pp. 1–6, IEEE, 2010.

[6] V. Petrov, A. Pyattaev, D. Moltchanov, and Y. Koucheryavy, "Terahertz band communications: Applications, research challenges, and standardization activities," in *2016 8th International Congress on Ultra Modern Telecommunications and Control Systems and Workshops (ICUMT)*, pp. 183–190, IEEE, 2016.

[7] P. Boronin, V. Petrov, D. Moltchanov, Y. Koucheryavy, and J. M. Jornet, "Capacity and throughput analysis of nanoscale machine communication through transparency windows in the terahertz band," *Nano Communication Networks*, vol. 5, no. 3, pp. 72–82, 2014.

[8] I. F. Akyildiz and J. M. Jornet, "Realizing ultra-massive MIMO (1024× 1024) communication in the (0.06–10) terahertz band," *Nano Communication Networks*, vol. 8, pp. 46–54, 2016.

[9] V. Petrov, M. Komarov, D. Moltchanov, J. M. Jornet, and Y. Koucheryavy, "Interference and SINR in millimeter wave and terahertz communication systems with blocking and directional antennas," *IEEE Transactions on Wireless Communications*, vol. 16, no. 3, pp. 1791–1808, 2017.

[10] V. Petrov, D. Moltchanov, Y. Koucheryavy, and J. M. Jornet, "The effect of small-scale mobility on terahertz band communications," in *Proceedings of the 5th ACM International Conference on Nanoscale Computing and Communication*, pp. 1–2, 2018.

[11] V. Petrov, D. Moltchanov, Y. Koucheryavy, and J. M. Jornet, "Capacity and outage of terahertz communications with user micro-mobility and beam misalignment," *IEEE Transactions on Vehicular Technology*, 2020.

[12] S. K. Moorthy and Z. Guan, "Beam learning in MmWave/THz-band drone networks under in-flight mobility uncertainties," *IEEE Transactions on Mobile Computing*, 2020.

[13] M. Polese, L. Bertizzolo, L. Bonati, A. Gosain, and T. Melodia, "An experimental mmWave channel model for UAV-to-UAV communications," in *Proceedings of the 4th ACM Workshop on Millimeter-Wave Networks and Sensing Systems*, pp. 1–6, 2020.

[14] E. N. Papasotiriou, J. Kokkoniemi, A.-A. A. Boulogeorgos, J. Lehtomäki, A. Alexiou, and M. Juntti, "A new look to 275 to 400 GHz band: Channel model and performance evaluation," in *2018 IEEE 29th Annual International Symposium on Personal, Indoor and Mobile Radio Communications (PIMRC)*, pp. 1–5, IEEE, 2018.

[15] A.-A. A. Boulogeorgos, E. N. Papasotiriou, and A. Alexiou, "Analytical performance evaluation of Thz wireless fiber extenders," in *2019 IEEE 30th Annual International Symposium on Personal, Indoor and Mobile Radio Communications (PIMRC)*, pp. 1–6, IEEE, 2019.

[16] A. B. Constantine *et al.*, "Antenna theory: analysis and design," *Microstrip Antennas, John Wiley & Sons*, 2005.

[17] Y. Liu, Y. Zhang, Y. Yao, and M. Zhong, "Laser point detection based on improved target matching method for application in home environment human-robot interaction," in *2018 11th International Workshop on Human Friendly Robotics (HFR)*, pp. 13–18, IEEE, 2018.

[18] A. Orsino, D. Moltchanov, M. Gapeyenko, A. Samuylov, S. Andreev, L. Militano, G. Araniti, and Y. Koucheryavy, "Direct connection on the move: Characterization of user mobility in cellular-assisted D2D systems," *IEEE Vehicular Technology Magazine*, vol. 11, no. 3, pp. 38–48, 2016.

[19] F. J. Massey Jr, "The kolmogorov-smirnov test for goodness of fit," *Journal of the American statistical Association*, vol. 46, no. 253, pp. 68–78, 1951.

[20] J. R. Bence, "Analysis of short time series: correcting for autocorrelation," *Ecology*, vol. 76, no. 2, pp. 628–639, 1995.

[21] W. Khreich, E. Granger, A. Miri, and R. Sabourin, "A survey of Techniques for Incremental Learning of HMM Parameters," *Information Sciences*, vol. 197, pp. 105–130, 2012.

[22] M. J. Gales, "Maximum Likelihood Linear Transformations for HMM-Based Speech Recognition," *Computer Speech & Language*, vol. 12, no. 2, pp. 75–98, 1998.

[23] S. Redner, *A Guide to first-passage processes*. Cambridge University Press, 2001.

[24] P. L. Krapivsky, S. Redner, and E. Ben-Naim, *A kinetic view of statistical physics*. Cambridge University Press, 2010.

[25] A. Stuart, M. G. Kendall, *et al.*, *The advanced theory of statistics*. Griffin, 1963.

[26] S. Andersen, "On the fluctuations of sums of random variables," *Math. Scand.*, vol. 1, pp. 263–297, 1953.

[27] W. Willinger, V. Paxson, R. H. Riedi, and M. S. Taqqu, "Long-range dependence and data network traffic," *Theory and applications of long-range dependence*, pp. 373–407, 2003.